Flat Lens-in-Package Architecture Using Multi-Axis Machining in D-Band

van Rooijen, Nick; Alonso-DelPino, Maria; Bueno, Juan; Llombart, Nuria

DOI
10.1109/OJAP.2025.3613605

Publication date
2025

Document Version
Final published version

Published in
IEEE Open Journal of Antennas and Propagation

Received 14 July 2025; revised 6 September 2025; accepted 9 September 2025. Date of publication 22 September 2025; date of current version 24 November 2025.

Digital Object Identifier 10.1109/OJAP.2025.3613605

Flat Lens-in-Package Architecture Using Multi-Axis Machining in D-Band

NICK VAN ROOIJEN [1], MARIA ALONSO-DELPINO [1] (Senior Member, IEEE), JUAN BUENO [2], AND NURIA LLOMBART [1] (Fellow, IEEE)

[1]Terahertz Sensing Group, Microelectronics Department, Delft University of Technology, 2628 CD Delft, The Netherlands
[2]Electronic Circuits and Architectures Group, Microelectronics Department, Delft University of Technology, 2628 CD Delft, The Netherlands

CORRESPONDING AUTHOR: N. VAN ROOIJEN (e-mail: n.vanrooijen@tudelft.nl)

This work was supported by the Huawei Technologies Sweden AB.

ABSTRACT This work presents an electrically-small lens that has been redesigned towards a flat interface. This way, the lens is easier to integrated, compared to an earlier introduced spherical core-shell lens concept. The lens is created from a single dielectric host material by conformally machining holes into the material. In this process, two artificial dielectric layers are created; The first layer is used for anti-reflection purposes, whereas the second is used to convert the spherical interface to a flat interface. The two layers enable the use of holes with lower aspect ratio drilling, compared to classical gradient-index lenses. The lens is designed to operate in the 140-170 GHz bandwidth, and a prototype with height of only 2.2 mm and diameter of 6.6 mm was fabricated and characterize. The prototype is small enough to fit in many integrated circuit packages. The flat lens was compared to a non-flat core lens in terms of pattern quality, return loss and dielectric loss, with only negligible performance degradation.

INDEX TERMS Antennas, flat lens, D-band.

I. INTRODUCTION

PROGRESS in Radio Frequency Integrated Circuit (RFIC) technologies has enabled wireless communications, sensing, and radar applications to extend into the D-band frequency range (110–170 GHz). This extension is of particular interest due to the availability of large portions of unlicensed spectrum, characterized by low atmospheric absorption [1]. The increased bandwidth facilitates higher data throughput, while the correspondingly shorter wavelengths enable the design of more compact antenna systems.

Despite these advantages, operating at D-band frequencies presents several challenges, including increased free-space path loss, diminished RF transmit power, and large overall system losses. Collectively, these factors contribute to a reduction in the overall system link budget. Mitigation of these issues at high frequencies requires the deployment of high-gain antennas to maintain system performance.

One RF system architecture utilizing high-gain antennas is the Fly's-Eye antenna system, first introduced in [2]. Operating within the D-band frequency range, this system employs a sparse lens array configuration to achieve high-gain, multi-beam coverage. To function effectively, the system requires antenna elements with gains exceeding 30 dBi and bandwidths greater than 20% [3].

To meet these criteria, recent work led to development of an integrated core-shell lens antenna [4], shown in Fig 2. The integration of such lens is shown conceptually in Fig. 1, indicating its complex assembly of the dual lenses. The design incorporated an electrically small core lens composed of dense thermoplastic material, surrounded by a larger shell lens made of low-permittivity material. The shell lens enhanced the antenna gain whilst maintaining low dielectric losses, whereas the compact core lens improves the front-to-back ratio and preserves the spherical wavefront shape. This core-shell lens configuration demonstrated good antenna performance in [4], achieving a bandwidth of approximately 30% and insertion losses below 2 dB, rendering it suitable for high-frequency applications.

Unfortunately, the dual-lens fabrication and assembly was a difficult process. The precise alignment required between the concave shell lens and convex core lens surfaces required tight tolerances. The potential for misalignment orientation and position is emphasized in Fig. 2b. These misalignments could result in an additional air gap between the two lenses,

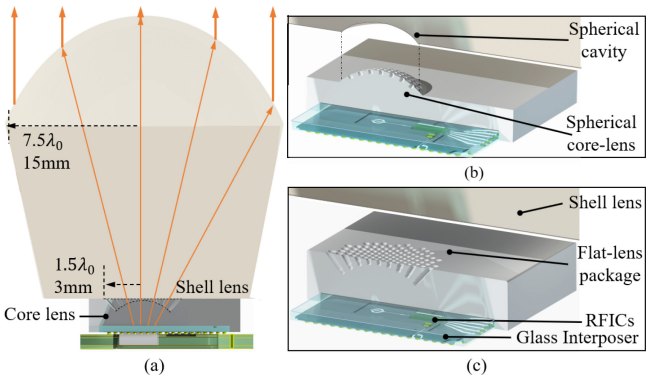

FIGURE 1. (a) Conceptual integrated core-shell lens antenna cross-sectional view. (b) Zoomed-in view of the spherical core lens interface with the spherical shell lens cavity. (c) proposed flat core lens for easier integration with the shell lens.

leading to pattern degradation and/or increased S_{11}. These effects add to the already intricate tolerating requirements of the assembly, leading to high-cost machining. For these reasons, a design of a flat core lens would be highly beneficial. A flat lens architecture furthermore permits the lateral movement of such lens underneath a shell lens, thereby enabling lens scanning, as in [5].

A common design for flat lenses is the use of Gradient Index (GRIN) refractive index lenses. A popular technique to fabricate flat lenses is by GRIN lenses is the use of additive manufacturing [6], [7]. Recent works have demonstrated 3D printed GRIN lenses even up to sub-THz domain [8], [9], [10]. However, the choice of materials for additive manufacturing is often limited, as the materials need to be both suitable for printing and the RF application. By contrast, CNC machining offers great flexibility in the material choice. In this technique, air cavities are CNC milled inside a host material, thereby creating a GRIN structure [11]. However, drilling unit cells for beyond 100GHz is challenging, due to the high aspect ratio drilling and the large number of holes (>1000) required. Finally, in [12], a technique involving a stratification of stacked PCBs was used to shape GRIN lenses. Unfortunately, at D-band frequencies, the unit cells become too small for the PCB tolerances to be a reliable solution. Also, a large number of stacked PCBs is required to create electrically large lenses. For a detailed discussion on related antenna designs, please refer to [4]. It is due to these challenges that a novel architecture for flat lenses is required that addresses current shortcomings.

In this work, we propose a compact flat lens made of dense thermoplastics using a novel design concept. Its early stage design was presented earlier in [13]. The proposed spherically conformal design is illustrated schematically in Fig. 4a. Such design conserves the spherical wavefront (i.e., not enhancing the directivity). The host dielectric material is modified via conformal machining of holes (Fig. 4b), resulting in two artificial dielectric layers within the compact lens structure. This topology enables a compact design that minimizes dielectric losses. The resulting flat core lens has

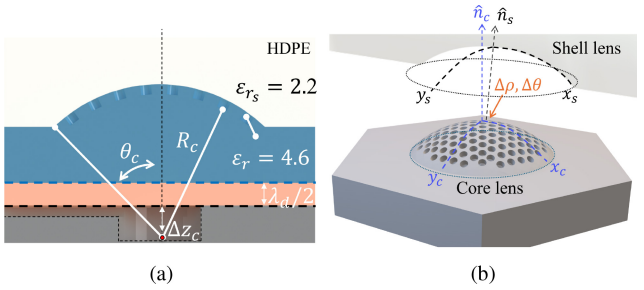

FIGURE 2. Cross-sectional view of (a) the spherical core lens, taken from [4], and (b) a 3D view of the same spherical lens. (b) furthermore indicates the potential for misalignment in orientation between the two lens interfaces. For orientation, there is the misalignment in lens normals $\hat{n}$, written as $\Delta\theta$, and in position between x, y center coordinates of the two lenses, written as $\Delta\rho$.

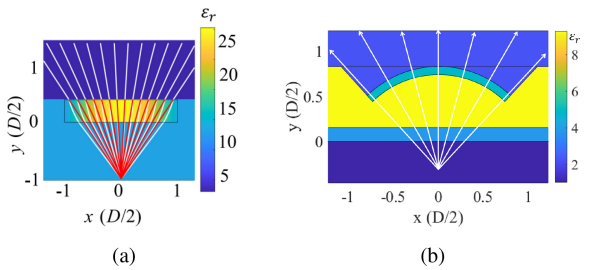

FIGURE 3. Comparison of the material effective permittivity distribution between (a) the GRIN lens of [15] and (b) the proposed flat core-shell lens.

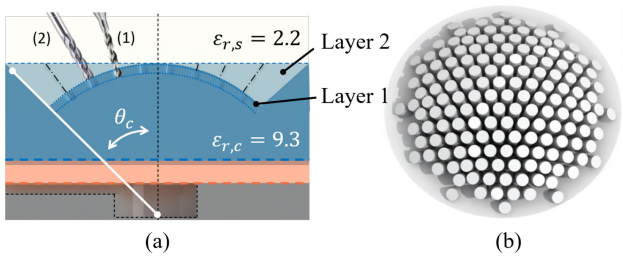

FIGURE 4. (a) The same core lens as in [4], but now adapted to a flat interface using an effective $\varepsilon_{r,s}$ permittivity. The two artificial dielectric layers are indicated. The two machining steps have been indicated. (b) Indication of the conformal drills required to shape the internally conformal flat lens.

a thickness of only 2.2 mm (1.13 λ_0, where λ_0 is the wavelength in free-space).

In parallel, a variation for the spherical design is proposed, by introducing a vertical extension of the lens feed with respect to its phase center. This extension enables an increase in the primary pattern directivity, and thereby unlocks low sidelobe level (SLL) performance.

This work addresses the design, optimization, fabrication, and characterization of this novel flat lens topology. The simulation methodology used to create and refine the lens design is detailed, followed by the fabrication process using multi-axis machining. Finally, the performance of the fabricated antenna prototype is validated through a set of antenna measurements.

II. FLAT LENS DESIGN

Commonly, GRIN lenses are used to create a flat lens interface using well-known theoretical frameworks [14].

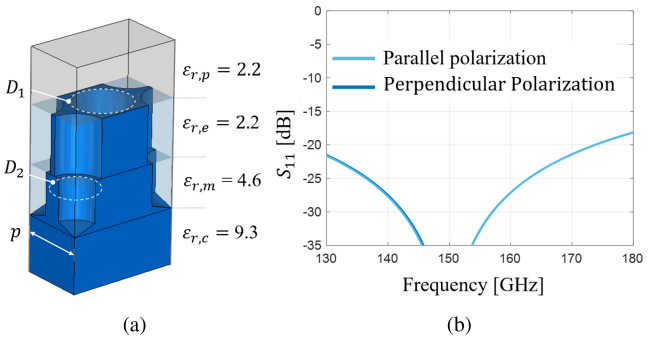

FIGURE 5. (a) Unit-cell of the matching layer. The optimized geometry has a matching layer diameter D_2 of 250 μm, effective permittivity layer diameter D_1 of 320 μm, and periodicity p of 360 μm ($\approx \lambda_d/4$). (b) The resulting S_{11} performance of the optimized unit cell.

In [15], a GRIN lens was designed to synthesize the core lens of [4], which was implemented on a PCB stack-up with thickness T. For such a design, the maximum required permittivity, which is proportional to a factor $1/T$, was $\varepsilon_{r,max} = 25$, as shown in Fig. 3a. Increasing T of the GRIN would lower this maximum permittivity, but also implies higher aspect ratio drilling and/or more PCB layers. Such type of GRIN lens implemented in dense thermoplastics with the same dimensions as [4], would need a permittivity of around 18, which increases not only the ohmic loss but also the fabrication challenges due to the reduction in the unit cell sizes.

In this work, 5-axis conformal machining is used to enable a flat core lens with a thickness of only 2.2 mm (1.13 λ_0) using a lower permittivity $\varepsilon_{r,c} = 9.3$ dielectric material. The main scope of the spherical core lens of [4] was to conserve the spherical wavefront that transitions between the core and shell lenses. The design is shown in Fig. 3b, and uses only three permittivity values: A host material with $\varepsilon_{r,c} = 9.3$ for the spherical core lens, $\varepsilon_{r,m} = 4.6$ for the matching layer and $\varepsilon_{r,e} = 2.2$ for the effective permittivity of the shell lens. Both $\varepsilon_{r,m}$ and $\varepsilon_{r,e}$ are obtained by removing part of the host dielectric material via the conformal holes. The detailed lens topology will be explained in the next sections.

A. FLAT LENS TOPOLOGY

The proposed novel flat lens concept is shown in Fig. 4a. The lens is made of PREPERM ($\epsilon_{r,c}$=9.3, tan$\delta = 0.005$), and internally has the same electrically small ($\approx 3\lambda_0$) spherical core lens including matching layer as in [4], shown in Fig. 2. However, a key difference is that now, instead of milling a spherical surface, the PREPERM material left with a flat interface by CNC machining an effective permittivity equal to the HDPE medium ($\epsilon_{r,s} = 2.2$, $tan\delta = 0.0003$). This enables the core lens to have an 'electrically' spherical interface, that is physically flat. This flat interface does not suffer from the same misalignment penalties as the spherical lens of Fig. 2b. A shift in position will only impact lens scanning, but has negligible impact on S_{11}. Finally, the orientation misalignment $\Delta\theta$ can be further mitigated due to the flat interfaces.

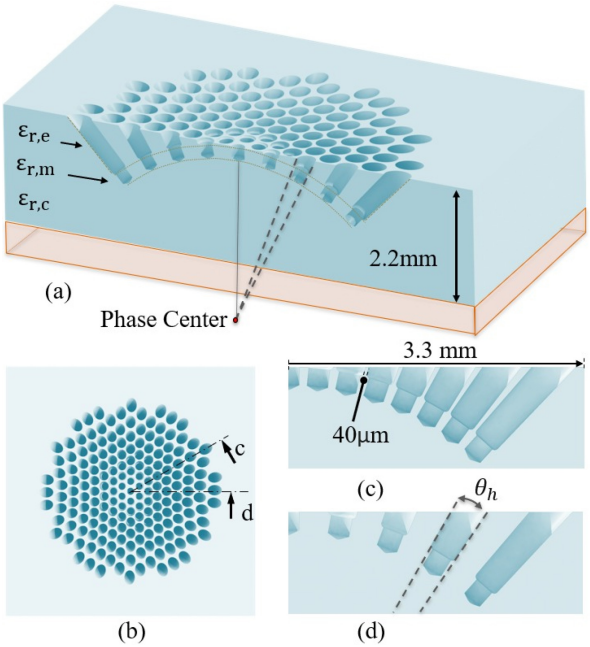

FIGURE 6. (a) Proposed flat core-lens prototype in cross-sectional view, indicating the different permittivity layers. (b) Top view of the flat core lens, with the cross-sectional views assigned in (c) and (d).

Fabrication of the artificial dielectric media is performed in a two-step approach, shown in Fig. 4b. First, like in [4] (Fig. 6a) the matching layer with effective $\epsilon_{r,m} = 4.6$ is drilled conformally with a 5-axis CNC machine, using a standard 250 μm drill bit. Next, the layer with effective $\epsilon_{r,e} = 2.2$ will be milled using the same periodicity as the previous layer, but with a slightly larger hole size. A conical taper originating from the antenna phase center was applied to the hole diameters, to keep the same volumetric fill ratio as the wave expands spherically. Although the conical hole milling provides a more constant $\epsilon_{r,eff}$, its machining is also more time-consuming than drilling of cylindrical holes. However, due to the electrically small size of the core lens, both conical and cylindrical holes could work, as the spherical spreading has only limited impact. In our proposed prototype, conically spreading holes were chosen for completeness.

With the fabrication process in mind, the next step was to derive the dimensions for the conformally drilled holes.

B. UNIT-CELL SIMULATIONS

To simulate the performance of the medium with effective permittivities, a Floquet-mode unit cell was used, shown in Fig. 5a. First, the matching layer situated between the ϵ_r=9.3 and $\epsilon_{r,e} = 2.2$ materials was designed nearly identical to [4], with a fixed hole diameter of 250 μm, period of $\approx$ 360 μm (variable) and depth of 255 μm ($\lambda_d/4$). This produces an $\epsilon_{r,m}$ of 4.6. Then, the milled layer with aimed effective permittivity of 2.2 was added in between the HDPE and matching layer. The structure was optimized by minimizing the S_{11} when iterating over the hole diameter and periodicity. The optimized S_{11} is shown in Fig. 5b, presenting

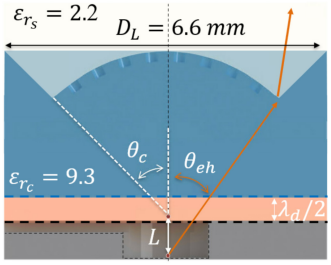

FIGURE 7. Geometry of the extended hemispherical lens. The extension is described by parameter *L*, as seen from the phase center. Except for this extension, the lens is identical to Fig. 4.

< 20 dB reflection coefficient for both parallel and perpendicular directions. The good dual-polarized performance implies not only that circularly-polarized feeding antennas can be used, but also that during the integration of the lenses, any rotational misalignment will not degrade antenna performance. The optimized performance was obtained using the dimensions stated in the caption of Fig. 5.

C. SPHERICAL FLAT LENS DESIGN

Once the unit cell was optimized, the effective permittivity layer was designed conformally to the spherical core lens surface. The subtended angle $\theta_c = 45°$ was kept similar to [4]. A cross-sectional view of the designed flat core lens is shown in Fig. 6b. The different layers are indicated inside the 2.2 mm thick lens, and the internal spherical core is visible. A top-view is presented in Fig. 6b, where all holes are visible in the hexagonal layout. The presented core-shell lens solution only requires 170 holes to synthesize both the matching layer and the effective permittivity layer. This in contrast to GRIN lenses found in literature with > 1000 drills ([11]), that operate < 100 GHz. Fig. 6b also indicates two cross-sectional lines, shown in Fig. 6c and 6d for 30° and 0° hexagonally symmetric cutting planes, respectively. The 30° cross-section represents the worst-case scenario with a minimum wall thickness between two adjacent holes of only 40 μm. However, due to the hexagonal layout, the wall thickness gradually increases until its maximum at 0° cross-sections. Also shown in Fig. 6a and d is the conical tapering that is applied to the holes. This means that the hole size is spherically increasing in size, with a fixed angle θ_h, with the sphere radius coincident with the phase center. This is fabricated by milling an increasingly larger hole size from the phase center, thereby creating a conically-shaped hole. This method is applied to keep the same volumetric fill ratio as the wave expands spherically.

D. EXTENDED HEMISPHERICAL FLAT LENS

An additional degree-of-freedom can be introduced in the flat lens design by including a vertical extension in the flat lens profile. Such design is a popular technique to enhance lens directivity [16]. This extended hemispherical geometry is shown in Fig. 7, where the vertical extension is dictated by parameter *L*. The hemispherical part of the lens

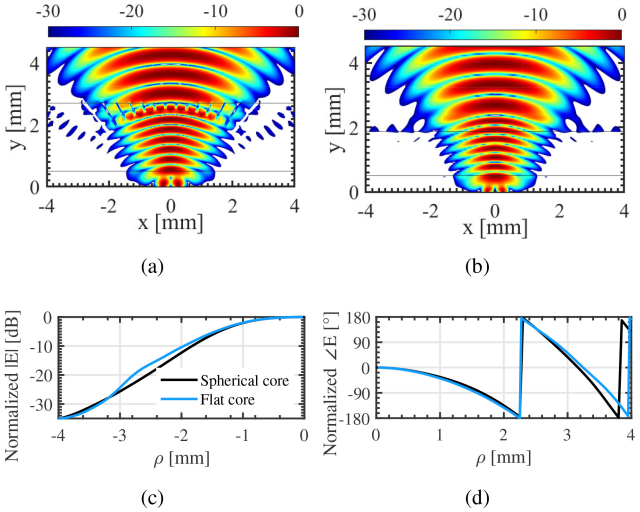

FIGURE 8. (a) Full-wave simulation of the normalized E-field (in dB) propagating at 155 GHz through the core lens. (b) The comparison to the same E-field propagating through the spherical core lens of [4]. (c) The comparison of the normalized near-field E-field amplitude at y = 3 mm between the spherical and the core lens. (d) The same comparison, but now in phase.

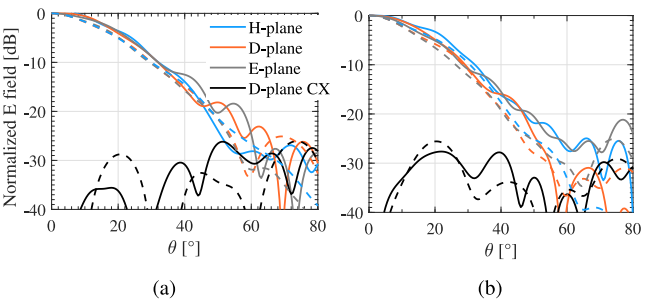

FIGURE 9. The primary patterns inside the infinite HDPE medium at 150 GHz (a) and 170 GHz (b) in solid, respectively. They are compared with the patterns of the spherical lens (in dashed). The D-plane CX represents the cross-polarization in the 45° plane, normalized to the co-polarized component at broadside. Both figures share the same y-axis.

is kept the same as in the non-extended lens. By choosing different values of *L*, different lens focusing capabilities can be selected.

In this work, an extension of $L = 1.45$ mm ($0.75\ \lambda_0$) was chosen, as a compromise between the SLL reduction and the lens spillover. The core lens subtended angle θ_c is kept the same 44° as the spherical flat lens. Therefore, the subtended angle θ_{eh} is reduced to 31.8 °. This way, Increasing the lens extension whilst keeping the same lens geometry increases lens spillover loss. However, this effect could be decreased by increasing the lens truncation angle θ_{eh} further (See Fig. 7).

III. SIMULATION RESULTS

A. CONFORMAL FLAT LENS

The design was simulated in a full-wave CST microwave studio solver. Similar to [4], the lenses were fed by a double-slot that is lithographically printed on a glass substrate, acting in turn as a leaky-wave feeding antenna.

Fig. 8 compares the 155 GHz E-fields propagating through the flat core lens (a) and spherical core lens

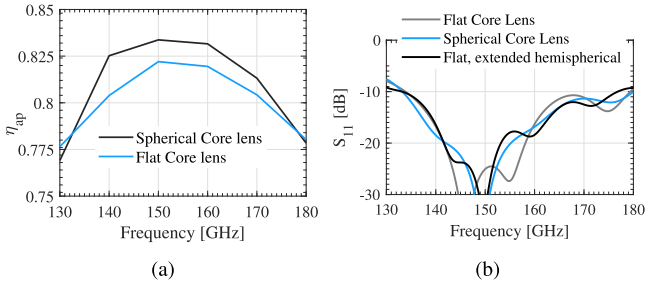

FIGURE 10. **(a) The flat lens aperture efficiency compared to the spherical lens. (b) S_{11} comparison of flat and spherical core lenses.**

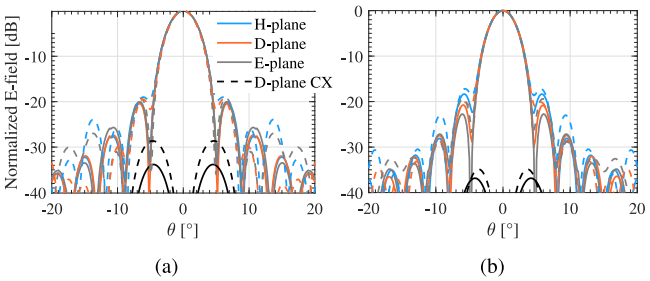

FIGURE 11. **Free-space secondary patterns derived using the GO/FO tool of [17] for (a) 150 GHz and (b) 170 GHz, comparing the flat lens (solid) versus the spherical lens (dashed). Both figures share the same y-axis.**

(b) interfaces. Horizontal lines have been added to indicate the core lenses. Both interfaces conserve the spherical wavefront as the material changes from dense thermoplastic to low-density HDPE. The flat lens has some stray radiation towards ± 60° angles, most likely caused by the reflections at the outer edges of the effective permittivity layer. However, its amplitude is at ≈ -30 dB w.r.t. the maximum E-field found at the center. Finally, Fig. 8c,d compares the amplitude and phase at the near-field at y = 3 mm. Both lenses show near-identical behavior in both metrics.

The primary patterns in infinite HDPE medium of both spherical and flat core lenses are compared in Fig. 9. Only limited pattern degradation occurs when switching to the new topology. As can be observed in Fig. 8a, at angles close to the edge of the effective permittivity layer, the performance degrades because the material no longer provides the $\varepsilon_{r,e}$ = 2.2 effective medium condition. This most likely causes an increase in radiation at large angles away from bore sight (> 50°), as visible in Fig. 9. A larger θ_{core} could help mitigate the problem, at the cost of increased machining time. As in [4], the pattern quality is quantified in the aperture efficiency η_{ap}, where the patterns in infinite $\varepsilon_{r,p}$ medium are analyzed using the Fourier optics tool of [17]. The resulting η_{ap}, representing the shell lens illumination efficiency, is shown in Fig. 10a. The shell lens subtended angle is set to 37° to optimize η_{ap}. A small difference of only 1-2% is observed when comparing the flat and spherical core lenses.

The antenna S_{11}, shown in Fig. 10, has similar behavior for both lenses, indicating that the flat lens is also able to present a near-reflection-less interface to the feeding antenna. Furthermore, we note that the simulated dielectric

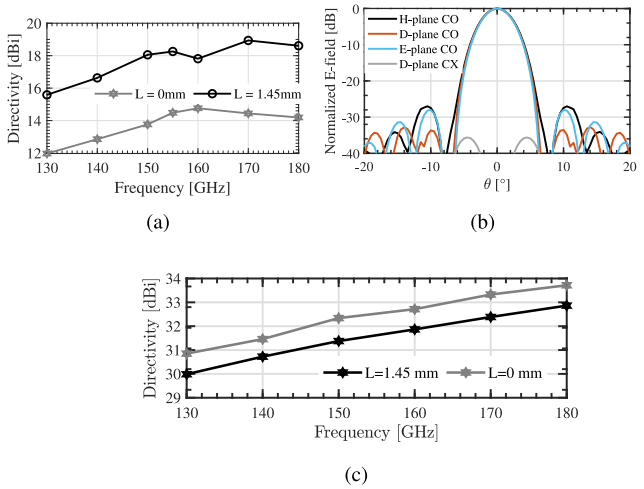

FIGURE 12. **(a) Full-wave simulated primary pattern directivity of the flat lens without extension (L=0), and the flat lens with 1.45 mm extension. (b) The resulting free-space secondary pattern at 155 GHz, with the reduced SLL, compared to non-extended lens. (c) The comparison in simulated free-space far-field directivity of the two lenses.**

loss increases from 0.23 dB to 0.36 dB, when switching from the spherical to the flat core lens, due to increasing the wavefront path through lossy dielectric material.

To conclude, Fig. 11 shows the secondary patterns in free space of the flat core and shell lenses, obtained using the GO/FO tool of [17]. The resulting patterns have good azimuthal symmetry, indicating that the flat core lens provides good rotational symmetry for the wavefronts. Furthermore, no large differences between the flat lens and spherical lens are observed.

B. EXTENDED HEMISPHERICAL FLAT LENS

Simulating the extended hemispherical lens was done in the same way as the non-extended variant, using a full-wave solver. The effect of the extension becomes apparent when analyzing the lens primary patterns (e.g., in infinite ε_r=9.3) for their directivity. This is shown in Fig. 12a. The extension enables an additional 3 to 4 dB of directivity. This implies that the shell lens is illuminated with a more tapered amplitude distribution, compared to the non-extended lens. The result is apparent in the far-field patterns, shown in Fig. 12b. The SLL is significantly decreased by >8 dB, when compared to the conformal lens patterns of Fig. 11. The penalty is paid in main-beam directivity, calculated using [17], and compared in Fig. 12c. The difference in directivity between the $L = 0$ mm and $L = 1.45$ mm antennas is 0.97 dB at the central frequency. Finally, Fig. 10b shows that simulated S_{11} behavior is similar for the extended hemispherical lens and the non-extended lens.

IV. FLAT LENS PROTOTYPE MEASUREMENTS AT D-BAND

We fabricated the conformal flat lens to experimentally test the concept and design, and to make the direct comparison to the spherical lens of [4]. The conformal flat

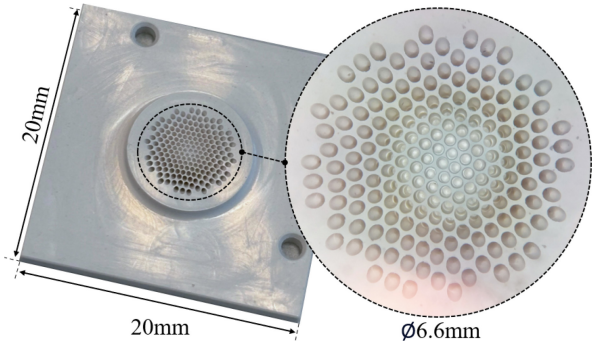

FIGURE 13. Fabricated prototype of the flat lens. The inset shows in more detail the drilled holes in the hexagonal grid layout.

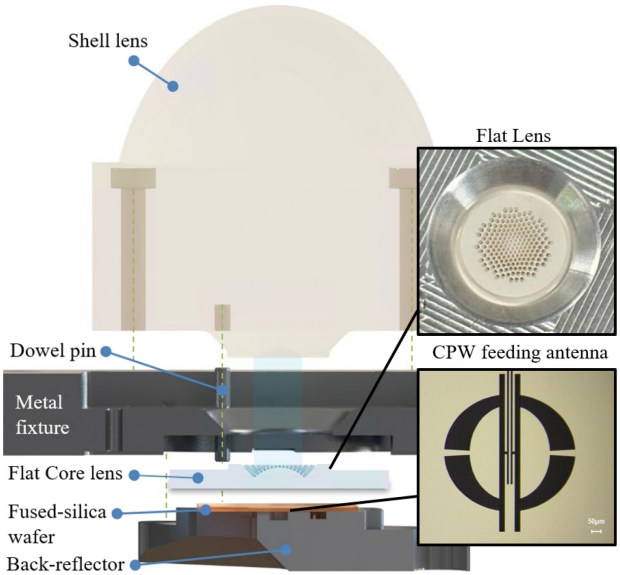

FIGURE 14. Exploded view of the prototype assembly, the same as in [4], except that its spherical core lens is now replaced by the flat lens. The insets show the photographs of the flat lens inside the assembly and the CPW feeding antenna from [4].

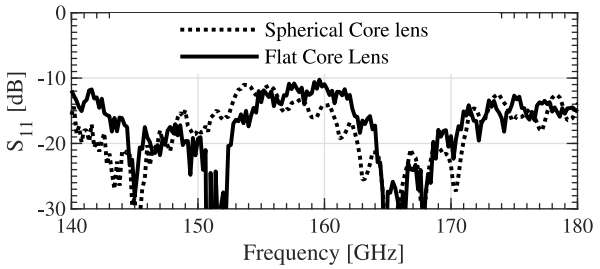

FIGURE 15. Measured S_{11} of the flat lens (solid) and the spherical lens (dashed).

lens prototype was fabricated using aforementioned 5-axis machining techniques. The prototype is shown in Fig. 13. The 20 × 20 mm outline and the location of the dowel pins is exactly the same as in [4]. This enables the compatibility of the prototype in the same integrated antenna assembly. A detailed view of the lens is shown in the inset. Although small deformations in periodicity and uniformity are visible at the center of the lens, the overall fabrication process is according to specifications.

To validate the simulated antenna performance, a set of measurements was performed with the fabricated prototype. The prototype is added to the same dual-lens assembly of [4], as shown in Fig. 14. The feeding antenna, shown in the inset of Fig. 14, is a lithographically printed double-slot antenna with coplanar waveguide (CPW) transmission lines, as taken from [4]. The measurement setup is identical to the one presented in [4]: A near-field measurement setup with a 45° mirror, that is used to convert the probe fed radiation from the veritcal towards the horizontal plane. More details can be found in [18]. Because the setup and the flat conformal lens design are identical to [4], we can directly compare the measured results to those obtained with the spherical core lens.

Fig. 15 shows the measured antenna reflection coefficient of the flat lens, compared to the spherical lens. No time-gating is applied, as in [4]. Contrary to Fig. 10, the measurements include the CPW transmission lines. The two measurement sets indicate fair agreement, although the flat core lens introduces some additional ripples.

Next, the antenna patterns were obtained by measuring the 2D near-fields, and subsequently applying a near-field to far-field conversion. Again, the measurement setup and 2D scanning plane were kept as identical as possible to [4], to allow for fair comparison.

Fig. 16 shows the far-field patterns of the flat lens (solid), compared to the spherical lens of [4] (dashed). Three main observations can be made. First, good agreement in the main beam pattern is obtained, although a minor shifting in scanning direction has occurred for the flat lens (≈ -0.5°). This is likely due to a misalignment in the measurement setup. Second, a higher sidelobe is visible in the E-plane at $\theta \approx 10°$, particularly at 155GHz. This asymmetry is most likely caused by the interaction between the flat lens and the radiating CPW transmission line. This effect has not been included in the full-wave simulations of Section III due to computational intensity. Finally, we note in Fig. 16 that the cross-polarization levels show good agreement across frequency for both lenses.

Having obtained the measured far-field patterns, the directivity and gain can be extracted. The directivity follows directly from the patterns, and is shown in Fig. 17. The flat and spherical lenses show similar directivity values across frequency, although the former has somewhat higher rippling behavior. Deriving the far-field gain is more complex, and involves S-parameter calibration of the near-field setup. The process is the same as in [4], and explained in more detail there. The resulting far-field gain is also shown in Fig. 17. Oscillations of up to 1dB are observed for the flat lens, with overall values close to the spherical lens. Unfortunately, the CPW feeding line (inset of Fig. 14) has large radiation loss, as was found in [4]. This stray radiation could couple into the flat lens interface and cause unwanted radiation. An improved feeding line, such as the microstrip-based design of [4], could help resolve this issue. Despite these losses, decent radiation efficiency of around -3dB is obtained, in

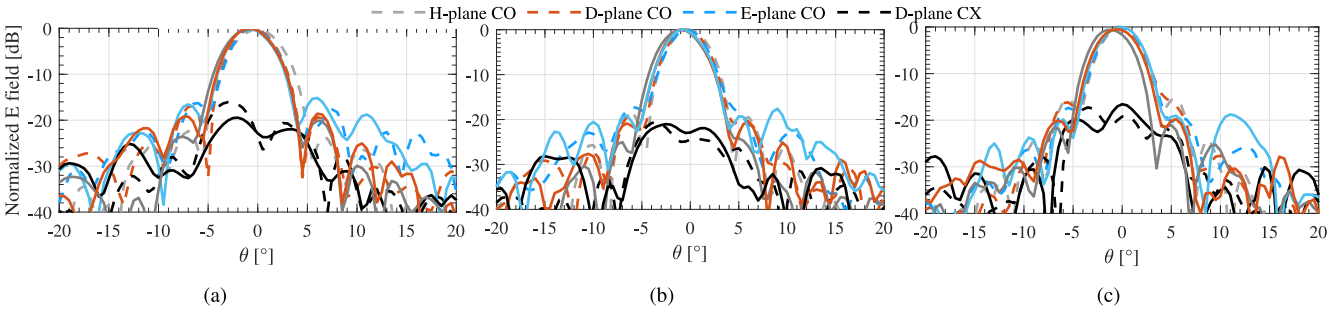

FIGURE 16. Measured free-space secondary patterns of the flat lens (solid) compared to the patterns of the spherical core lens (dotted). (a) 140 GHz (b) 155 GHz and (c), 170GHz comparing the flat lens (solid) versus the spherical lens (dashed).

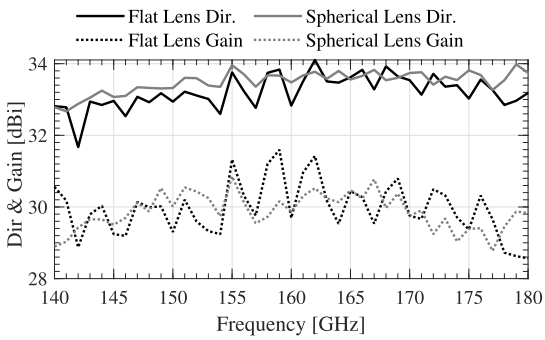

FIGURE 17. Measured far-field directivity.

close agreement to the value found in [4], where a feed loss of 1.2 dB was found, lens dielectric loss of only 0.5 dB, and the rest associated to spillover and front-to-back loss. This illustrates the advantage of the dual-lens design, where the compact core lens limits dielectric loss, and permits the transition to electrically-large lenses with negligible loss.

V. CONCLUSION

This work presented a design strategy for a novel compact flat lens using conformal CNC machining. The flat lens interface can be easily integrated to form a dual-lens architecture for a Fly's-Eye communication system. Two designs were illustrated, a conformal design similar to earlier work, and an extended hemispherical design for enhanced SLL performance.

The conformal flat lens was fabricated using 5-axis CNC machining techniques. The resulting compact flat core lens prototype has a height of only 2.2 mm (1.13 λ_0) and a diameter of 6.6 mm (3.4 λ_0). The compactness enables such lens to fit inside an RFIC encapsulation, hence providing the name lens-in-package.

The flat lens prototype was measured in the lab and compared to its spherical counterpart. Good agreement in the antenna reflection coefficient was obtained. Furthermore, overall good agreement in patterns, directivity and gain was obtained. The lens suffered from larger rippling effects than the spherical lens, due to unwanted radiation from the CPW line. Improved lens feeding design could help mitigate this problem.

ACKNOWLEDGMENT

The authors would like to thank Ulrik Imberg from Huawei for his assistance in this project.

REFERENCES

[1] T. S. Rappaport et al., "Wireless communications and applications above 100 GHz: Opportunities and challenges for 6G and beyond," *IEEE Access*, vol. 7, pp. 78729–78757, 2019.

[2] N. Llombart, D. Emer, M. A. Campo, and E. McCune, "Fly's eye spherical antenna system for future Tbps wireless communications," in *Proc. 11th Eur. Conf. Antennas Propag. (EuCAP)*, Paris, France, Mar. 2017, pp. 1–4.

[3] M. A. Campo, D. Blanco, S. Bruni, A. Neto, and N. Llombart, "On the use of fly's eye lenses with leaky-wave feeds for wideband communications," *IEEE Trans. Antennas Propag.*, vol. 68, no. 4, pp. 2480–2493, Apr. 2020.

[4] N. van Rooijen et al., "A core-shell lens for antenna on-package integration at D-band," *IEEE Trans. Antennas Propag.*, vol. 72, no. 8, pp. 6195–6208, Aug. 2024, doi: 10.1109/TAP.2024.3417628.

[5] S. Bosma, N. Van Rooijen, M. Alonso-Delpino, M. Spirito, and N. Llombart, "First demonstration of dynamic high-gain beam steering with a scanning lens phased array," *IEEE J. Microw.*, vol. 2, no. 3, pp. 419–428, Jul. 2022, doi: 10.1109/JMW.2022.3179953.

[6] S. Zhang, R. K. Arya, W. G. Whittow, D. Cadman, R. Mittra, and J. C. Vardaxoglou, "Ultra-wideband flat metamaterial GRIN lenses assisted with additive manufacturing technique," *IEEE Trans. Antennas Propag.*, vol. 69, no. 7, pp. 3788–3799, Jul. 2021, doi: 10.1109/TAP.2020.3044586.

[7] A. Paraskevopoulos, F. Maggiorelli, I. Gashi, C. D. Giovampaola, M. Albani, and S. Maci, "3-D printed all-dielectric GRIN lens antenna with an integrated feeder," *IEEE Open J. Antennas Propag.*, vol. 4, pp. 528–536, 2023, doi: 10.1109/OJAP.2023.3273488.

[8] Y. Guo, F. Meng, K. Ma, J. Ma, and Y. Luo, "A terahertz wide-angle beam-steering 3D-printed dual-polarized GRIN lens with planar focal surface," *IEEE Trans. Terahertz Sci. Technol.*, vol. 15, no. 3, pp. 519–525, May 2025, doi: 10.1109/TTHZ.2025.3539503.

[9] P. Kaděra et al., "Alumina 3-D printed wide-angle partial maxwell fish-eye lens antenna," *IEEE Antennas Wireless Propag. Lett.*, vol. 23, no. 7, pp. 2051–2055, Jul. 2024, doi: 10.1109/LAWP.2024.3378754.

[10] J. Chen, S. X. Huang, K. F. Chan, G. B. Wu, and C. H. Chan, "3D-printed aberration-free terahertz metalens for ultra-broadband achromatic super-resolution wide-angle imaging with high numerical aperture," *Nat. Commun.*, vol. 16, p. 363, 2025. [Online]. Available: https://doi.org/10.1038/s41467-024-55624-w

[11] M. Imbert, A. Papió, F. De Flaviis, L. Jofre, and J. Romeu, "Design and performance evaluation of a dielectric flat lens antenna for millimeter-wave applications," *IEEE Antennas Wireless Propag. Lett.*, vol. 14, pp. 342–345, 2015, doi: 10.1109/LAWP.2014.2363596.

[12] C. M. Coco Martin, W. Hu, and D. Cavallo, "Design of wide-band flat artificial dielectric lenses at mmWave frequencies," *IEEE Trans. Antennas Propag.*, vol. 72, no. 2, pp. 1418–1428, Feb. 2024, doi: 10.1109/TAP.2024.3357992.

[13] N. van Rooijen, M. Alonso-delPino, and N. Llombart, "Flat lens concept using multi-axis machining for D-band core-shell lens-in-package integration," in *Proc. 20th Eur. Conf. Antennas Propag. (EuCAP)*, Stockholm, Sweden, pp. 3952–3956, Apr. 2025.
[14] F. Maggiorelli, A. Paraskevopoulos, J. C. Vardaxoglou, M. Albani, and S. Maci, "Profile inversion and closed form formulation of compact GRIN lenses," *IEEE Open J. Antennas Propag.*, vol. 2, pp. 315–325, 2021.
[15] W. Hu, C. M. Coco Martin, and D. Cavallo, "Design formulas for flat gradient index lenses with planar or spherical output wavefront," *IEEE Trans. Antennas Propag.*, vol. 72, no. 3, pp. 2555–2563, Mar. 2024, doi: 10.1109/TAP.2024.3363433.
[16] D. F. Filipovic, S. S. Gearhart, and G. M. Rebeiz, "Double-slot antennas on extended hemispherical and elliptical silicon dielectric lenses," *IEEE Trans. Microw. Theory Techn.*, vol. 41, no. 10, pp. 1738–1749, Oct. 1993, doi: 10.1109/22.247919.
[17] H. Zhang, S. O. Dabironezare, G. Carluccio, A. Neto, and N. Llombart, "A Fourier optics tool to derive the plane wave spectrum of quasi-optical systems [EM programmer's notebook]," *IEEE Antennas Propag. Mag.*, vol. 63, no. 1, pp. 103–116, Feb. 2021.
[18] N. Van Rooijen, M. Spirito, A. B. Triantafyllos, N. Llombart, and M. Alonso-delPino, "A near-field quasi-optical measurement technique for probe-fed high-gain backside-radiating antennas," in *Proc. IEEE/MTT-S Int. Microw. Symp.*, Washington, DC, USA, 2024, pp. 904–907, doi: 10.1109/IMS40175.2024.10600366.

NICK VAN ROOIJEN received the M.Sc. degree (cum laude) in electrical engineering from the Delft University of Technology (TU Delft), Delft, The Netherlands, in 2021, where he is currently pursuing the Ph.D. degree with Terahertz Sensing Group.

At TU Delft, his research focuses on the development of a Fly's eye lens array for high frequency communication applications. During the master's, he worked on a first-time demonstration of a high frequency scanning-lens phased-array. His research interests include the analysis, design, and measurement of integrated lens antennas and leaky-wave structures. He was the co-recipient of the Best Theory And Design Antenna Paper Award and was also nominated for the Best Applied Technology Antenna Paper Award, both at the 16th European Conference on Antennas and Propagation in 2022.

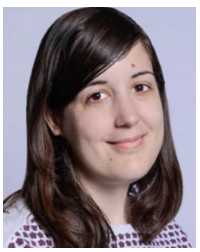

MARIA ALONSO-DELPINO (Senior Member, IEEE) received the degree in telecommunications engineering from the Technical University of Catalonia (UPC), Barcelona, Spain, in 2008, the M.S. degree in electrical engineering from the Illinois Institute of Technology, Chicago, IL, USA, in 2008, and the Ph.D. degree in signal theory and communications/electrical engineering from UPC in 2013.

From 2014 to 2015, she was as a Postdoctoral Researcher with the Technical University of Delft (TUDelft), Delft, The Netherlands. From 2015 to 2016, she was a NASA Postdoctoral Fellow with the Jet Propulsion Laboratory, Pasadena, CA, USA. From 20216 to 2020, she was a Member of the Technical Staff with the Sub-Millimeter Wave Advanced Technology Group of JPL/NASA. Since 2020, she is an Assistant Professor with TUDelft. Her research interests include millimeter and submillimeter-wave heterodyne and direct detection receiver technologies, antennas, and quasi-optical systems. She was the recipient of the 2014 IEEE Terahertz Science and Technology Best Paper Award and the Outstanding Reviewer Award of the IEEE Transactions on Terahertz Science and Technology in 2013. She has been nominated in 2021, 2022, and 2024, for best papers at the European Conference on Antennas and Propagation (EuCAP) and she received the Best Antenna Design Paper Award in 2022. She was awarded the IETE-Smt C Ranganayakamma Memorial Award in 2024. Since 2024, she has served as a Regional Delegate for European Association on Antennas and Propagation (EurAAP) of Region 5 Netherlands, Belgium, Luxemburg.

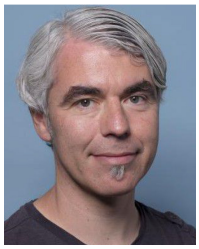

JUAN BUENO received the graduation degree in physics from the University of Cantabria, Santander, Spain, in 2003, and the Ph.D. degree in physics from the University of Leiden, Leiden, The Netherlands, in 2007.

During the Ph.D. degree, he studied quantum crystals at very low temperatures. From 2007 to 2008, he was a Postdoctoral Fellow with the University of California, San Diego, CA, USA, continuing his work on quantum crystals. In 2008, he switched his research topics and interests from fundamental physics to the study of superconducting devices. Until 2010, he was a Postdoctoral Researcher with Jet Propulsion Laboratory, Pasadena, CA, USA. During this time, he pioneered a new type of pair-breaking radiation detector, the quantum capacitance detector. After his time with JPL, he joined the Center for Astrobiology, Madrid, Spain, in 2010, working mainly on kinetic inductance detectors. He became an Instrument Scientist in 2012 with SRON, Netherlands Institute for Space Research, Leiden, The Netherlands, working on the development of KIDs for submillimeter wave and far IR space-based observatories. In 2021, he became a High-Frequency RF Engineer with ELCA Group, Technical University of Delft, Delft, The Netherlands, working on the XG sensing and communications laboratories. He has authored or co-authored more than 50 peer-reviewed papers, a fourth of them as the first author, and more than 40 peer-reviewed papers, almost a third of them as the first author. His research focuses on the development of over the air technology at submillimeter wave frequencies for detection and communication applications.

Dr. Bueno was the recipient of NASA Postdoctoral Position and the JAE-doc Grant.

NURIA LLOMBART (Fellow, IEEE) received the master's degree in electrical engineering and the Ph.D. degree in electromagnetics from the Polytechnic University of Valencia, Valencia, Spain, in 2002 and 2006, respectively.

During her master's degree studies, she spent one year with the Friedrich Alexander University of Erlangen Nuremberg, Erlangen, Germany, and worked with the Fraunhofer Institute for Integrated Circuits, Erlangen, Germany. From 2002 to 2007, she was with the Antenna Group, TNO Defense, Security and Safety Institute, The Hague, The Netherlands, was a Ph.D. student and afterward as a Researcher. From 2007 to 2010, she was a Postdoctoral Fellow with the SubmillimeterWave Advance Technology Group, Jet Propulsion Laboratory, California Institute of Technology, Pasadena, CA, USA. She was a "Ramón y Cajal" Fellow with the Optics Department, Complutense University of Madrid, Madrid, Spain, from 2010 to 2012. In 2012, she was with the THz Sensing Group, Technical University of Delft, Delft, The Netherlands, where she has been a Full Professor since 2018. She has co-authored more than 200 journal and international conference contributions in the areas of antennas and terahertz systems. She was the co-recipient of the H. A. Wheeler Award for the Best Applications Paper of 2008 in IEEE Transactions on Antennas and Propagation, the 2014 THz Science and Technology Best Paper Award of the IEEE Microwave Theory and Techniques Society, and several NASA awards. She was also the recipient of the 2014 IEEE Antenna and Propagation Society Lot Shafai Mid-Career Distinguished Achievement Award. In 2015, she was the recipient of European Research Council Starting Grant. She is a Board Member of the International Society of Infrared, Millimeter, and Terahertz Waves and, since 2023, an Editor in Chief of the IEEE Transactions on THz Science and Technology. In 2019, she was appointment IEEE Fellow for contributions to millimeter and submillimeter wave quasi-optical antennas.